nature communications

Article

https://doi.org/10.1038/s41467-024-54393-w

Programmable and rapid fabrication of complex-shape ceramics

Received: 16 April 2024

Accepted: 4 November 2024

Published online: 18 November 2024

Check for updates

Yao Shan[1,2,5], Xuemu Li[1,5], Wanjun Zhao[3,5], Xiaodan Yang[1,4], Yuanyi Wang[1], Zhuomin Zhang[1,4], Shiyuan Liu[1], Xiaote Xu[1] & Zhengbao Yang[1]

Shaping of ceramics is crucial. Current techniques cannot easily and rapidly shape ceramics without weakening their properties, especially for piezoceramics. We present an ultrafast ceramic shaping method that leverages thermomechanical fields to deform and sinter ceramic powder compacts into complex-shaped ceramics. The shape-forming process hinges on: (1) the implementation of a precise thermal field to activate optimal deformability, and (2) the application of sufficient mechanical loads to guide deformation. We employ a programmable carbon-felt Joule heater that concurrently function as mechanical carriers, effectively transferring applied loads to the ceramic powder compacts. Using this ultrafast shaping and sintering (USS) method, we fabricate barium titanate (BT) piezoceramics in twisted shape, arch shape and with micropatterns. The USS method is energy-friendly (requiring approximately 1.06 kJ mm^{-3}) and time-efficient (in several minutes level). Overall, the USS method offers an effective solution for shaping ceramics and extends them to 3D geometries with enhanced versatility.

Ceramics play essential roles in electronic devices, renewable energy technologies and components in extreme environments because of their robust mechanical, thermal and chemical properties[1–3]. Shaping is the key to bringing ceramic materials to widespread use components, especially for those functional ceramics that benefit from geometrical features. For example, a small curvature of a piezoceramic sheet can greatly improve the power output of the simplest energy-harvesting cantilever beam[4,5]. Furthermore, irregular geometries are ubiquitous in real objects that usually require coupling components with complex shapes[6–8]. The high hardness and brittleness of ceramic materials make the manufacturing time-consuming and challenging[9,10]. This severely limits the component geometries, confining ceramics to paradigms in which near-net and planar shapes are the only options. The conventional slip casting technique is typically used to form ceramics in complicated shapes[11,12]. However, the complicated demolding procedures, limited material composition and long drying time hinder the generalization of the slip casting. State-of-the-art ceramic shaping methods like injection molding and 3D printing particularly for producing ceramics with densified bodies[13,14] involve the fabrication and sintering of ceramic green specimens with a high content of polymer. However, removing polymers in these ceramic green specimens requires long-term exposure to high temperatures at low heating rates and the sintered ceramics often exhibit compromised performances[15]. Rapid, reliable, and cost-friendly ceramic shaping methods are thus in urgent demand.

The shaping conundrum has historically been one of the major impediments to the widespread use of ceramic materials. The shape formation of metals, glasses, and polymers by using their temperature-dependent states has been widely introduced in material processing handbooks, for instance, metals forging, glass blowing, and thermoforming of polymers. However, it is normally believed that large thermal deformation is not possible in brittle ceramic materials. The thermal-induced creep is a common phenomenon in crystalline solids[16–18] and could be instrumental in forming the shapes of ceramics

[1]Department of Mechanical and Aerospace Engineering, Hong Kong University of Science and Technology, Hong Kong, China. [2]Department of Chemistry, Purdue University, Indiana, USA. [3]State Key Laboratory of Explosion Science and Technology, Beijing Institute of Technology, Beijing, China. [4]Department of Mechanical Engineering, City University of Hong Kong, Hong Kong, China. [5]These authors contributed equally: Yao Shan, Xuemu Li, Wanjun Zhao.
e-mail: zbyang@ust.hk

(a typical kind of crystalline solid materials). Actually, the high-temperature creep and superplastic behaviors of ceramics have been experimentally and numerically studied since 1980s[19,20]. Substantial attempts have focused on uncovering the deformation mechanism and constructing corresponding constitutive equations. The creep deformation of ceramics is dominated by the diffusional creep that is favored at high-temperatures, low stresses and fine grain sizes[17,21]. Mechanistically, in diffusional creep, the deformation of grains occurs when the transport of atomic vacancies is biased by applied stresses. The creep rate in crystalline ceramics is low, and a large deformation ruptures ceramic specimens[17,22]. Based on the ceramics creep mechanism, direct thermal treatments to shape ceramics is not accessible.

This work presents a Joule heating based rapid ceramic shaping technique that works beyond the limited creep rate and deformations of ceramic materials[17,23]. We experimentally found that at an elevated temperature (before reaching the sintering temperature) and a proper stress state, we are able to deform ceramic green compacts without experiencing structural rupture[24]. This unexpected large deformation is achieved at a dynamic balance after the debinding and prior to crystalline formation, along with the sintering process. Both the thermal-induced viscosity and the particle-pore topology are responsible for the favorable deformability of ceramic green compacts at an elevated temperature. The particle-pore topologies of ceramic green compacts allow the movement and transposition of particles as well as pores. Therefore, ceramic green compacts exhibit approximately one-order higher strain rate compared with crystalline ceramics under similar stress state[16,25,26]. Based on this phenomenon, we develop the USS method. The USS exploits the Joule heating technique and the viscosity-based ceramic shaping mechanism. It morphs thermo-mechanical fields and provides a general method to fabricate complex-shaped ceramics. Using the USS method, we successfully fabricate piezoceramics in twisted shapes and structural ceramics in arch shapes. The as-fabricated complex-shape piezoceramics and structural ceramics showcase their potentials in serving as the actuator for pumping liquid and the armor for protecting or packaging electronics, respectively. This study paves a time-efficient and energy-friendly way for rapidly shaping ceramics, thus freeing ceramic components from geometrical limits.

Results

Working principle of the ultrafast shaping and sintering (USS) process

The USS process relies on the thermomechanical field engineering and fabricates complex-shaped ceramics while keeping their intrinsic material properties. In this process, the ceramic green compact (Fig. 1a) is placed in a morphing thermal field (Fig. 1b) to guide the bending and twisting of ceramic specimens; finally, after rapid sintering, we obtain the densified complex-shape ceramics (Fig. 1c). The USS hinges on the thermal-induced viscosity and particle-pore topology of ceramic green compacts. Specifically, the ceramic green compacts show poor deformability at low temperatures, while the viscosity activated at elevated temperature makes the compacts deformable (yellow shadow region in Fig. 1b ii). At the beginning of the shaping range, the particles are soft-linked via the Van der Waals force and the frictional force (Supplementary Fig. 1a i), meanwhile these pores provide particles with sufficient spaces to migrate. Further raising the temperature (near or approaching the sintering temperature) causes contact diffusion (Supplementary Fig. 1a ii) and grain growth (Supplementary Fig. 1a iii), which reinforces the connection between particles/grains. These strong bonds limit the relative motion between particles/grains, and therefore, in macro presentation, the densified ceramics show low deformability even at high temperatures. Actually, the thermal-induced viscosity has been exploited to fabricate curved ceramics without sacrificing performances[7,24]; however, attempts to rapidly and actively shape ceramics at high temperatures are unsuccessful because 1) the deformation is a time-dependent and slow; 2) the self-weight is the only mechanical-driven source. Taking BT piezoceramic as an example, the lightweight powder compacts can merely generate slight deformation by the gravitational force. Furthermore, the heating and shaping are conducted in conventional furnaces, which show large thermal inertia and inconvenient mechanical modulations.

Fabrication strategy of the USS process

As a demonstration of the USS process, we shape and sinter BT ceramics, a kind of lightweight piezoelectric ceramics. Following the principle (Fig. 1b), we first confirm the proper shaping temperature range (1220–1370 K) by the high-temperature thermomechanical analysis of the BT green compacts (see Supplementary Fig. 1 and

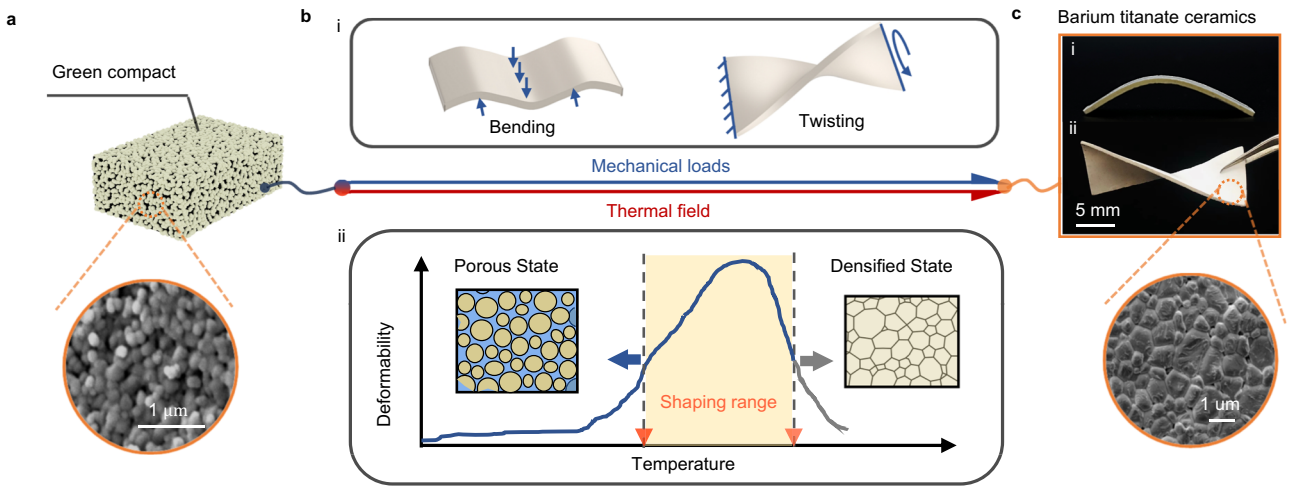

Fig. 1 | The ultrafast shaping and sintering (USS) process. a The green compact that exhibits high brittleness and poor processibility. **b** The working principle of the USS process that relies on the cooperation between the mechanical and thermal fields, where the blue and red arrows denote mechanical and thermal processes respectively. Specifically, two key points: (i) sufficient mechanical loads to guide the ceramic powder compacts; (ii) proper thermal field to activate the good deformability of the green compact. The porous-state ceramics comprises ceramic particles (yellow circles) and air gaps (blue area). **c** Photographs of the USS-fabricated arch-shape and twisted BT ceramics.

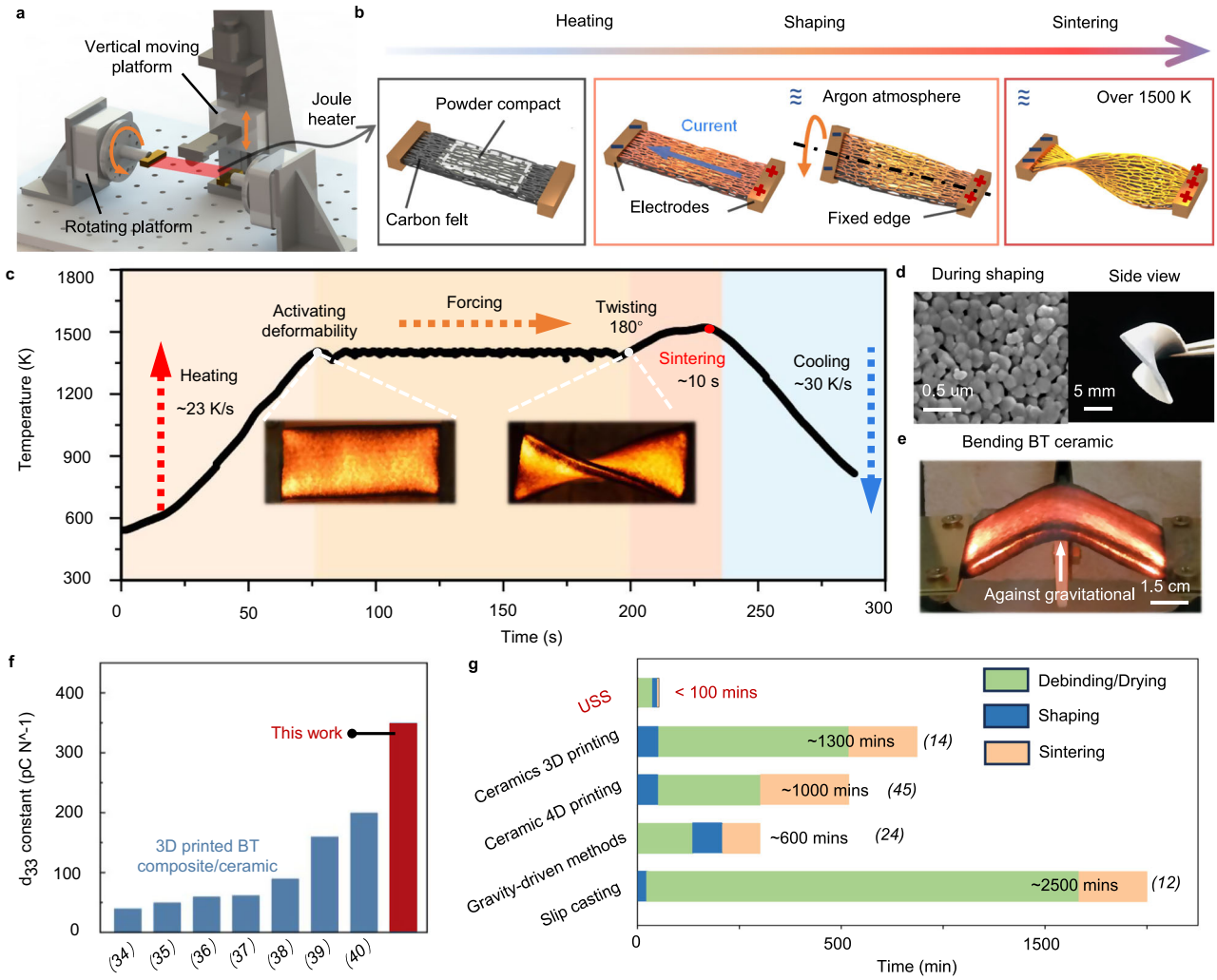

Fig. 2 | Operation and performance of the USS process. a Schematic of the USS platform, comprising three precision moving drivers and one carbon-felt Joule heater. **b** Schematic illustration of a typical USS process for twisting ceramics, in which the ceramic green compact is clamped by carbon felts and then heated for forming shapes before sintering to crystalline ceramics. **c** The temperature profile and the digital images of the processing element as well as USS specimen. The high heating and cooling rates of the USS process enable us to shape and sinter ceramics in a few minutes. **d** Photograph of the twisted BT ceramic and SEM images of the BT ceramic during twisting. **e** Digital image of processing the arch-shape BT ceramic where the powder compact is bent against gravity direction. **f** Comparison of piezoelectric constants d_{33} between the twisted BT ceramic presented in this study and current complex-shape BT-based piezoelectric materials ref. 34–40. **g** Comparison of the processing time of our USS method with those of existing ceramic shaping methods ref. 12,14,24,45.

Supplementary Note 1 for the details of the thermomechanical analysis). Recently, the carbon felts Joule heating method emerges as a promising route for ultrafast high-temperature material synthesis[1,27,28] and convenient heating profile modulation[29–31]. Moreover, the flexibility of the Joule heating method in thermal field formation allowed it smoothly integrate with other fabrication techniques for instance, 3D printing technique[32]. To apply the USS process, we use Joule-heated carbon felts combined with three precision moving platforms (Fig. 2a), which all are placed in an inert atmosphere (Argon). The low heat capacity of carbon felts allows us to form a thermal field in high ramping and cooling rates by directly passing current through them (Fig. 2b). The carbon felts also serve as the mechanical carrier to clamp specimens and transfer forces/deformations (Fig. 2b). To activate high deformability (Supplementary Movie 1), the BT powder compact is sandwiched between two pieces of Joule-heated carbon felt that rapidly form a uniform and stable thermal field (1400 K, left digital image in Fig. 2c), then driving the ceramic specimen twist (right digital image in Fig. 2c) by applying torsional deformation. The shaping stage is followed by ~20 s of temperature ramping and ~10 s of isothermal sintering (1520 K). Different from the gravity-based ceramic shaping strategy disclosed in our previous works, here we actively control the shape-forming process, overcoming the geometry and material selection restrictions caused by the gravity (driven force). For instance, the shape of the arch BT ceramic shown in Fig. 1c is formed via bending the powder compact against gravity direction (Fig. 2e and Supplementary Movie 2 for the bending process).

Performance evaluation of the USS process

The high temperature ramping rate and short sintering duration result in fine grain size of 1.2 ± 0.2 μm and a high relative density of ~96% (Supplementary Fig. 2a and Supplementary Fig. 2b). The twisted BT specimens also possess piezoelectric phase structure of the tetragonal phase (Supplementary Fig. 2c). We also measured the ferroelectric polarization versus electric field (*P*–*E*) loop (Supplementary Fig. 2d) and the strain–electric field (*S*–*E*) curve (Supplementary Fig. 2d) to evaluate the piezoelectric performance of the as-fabricated BT ceramics. The USS-fabricated BT ceramic exhibits typical piezoelectric properties with the remanent polarization of around 24 μC cm^{-2} and possesses butterfly-like shape strain–electric field (*S*–*E*) curve with the maximum compressive strain of around 0.4%. Furthermore, the USS-fabricated

https://doi.org/10.1038/s41467-024-54393-w

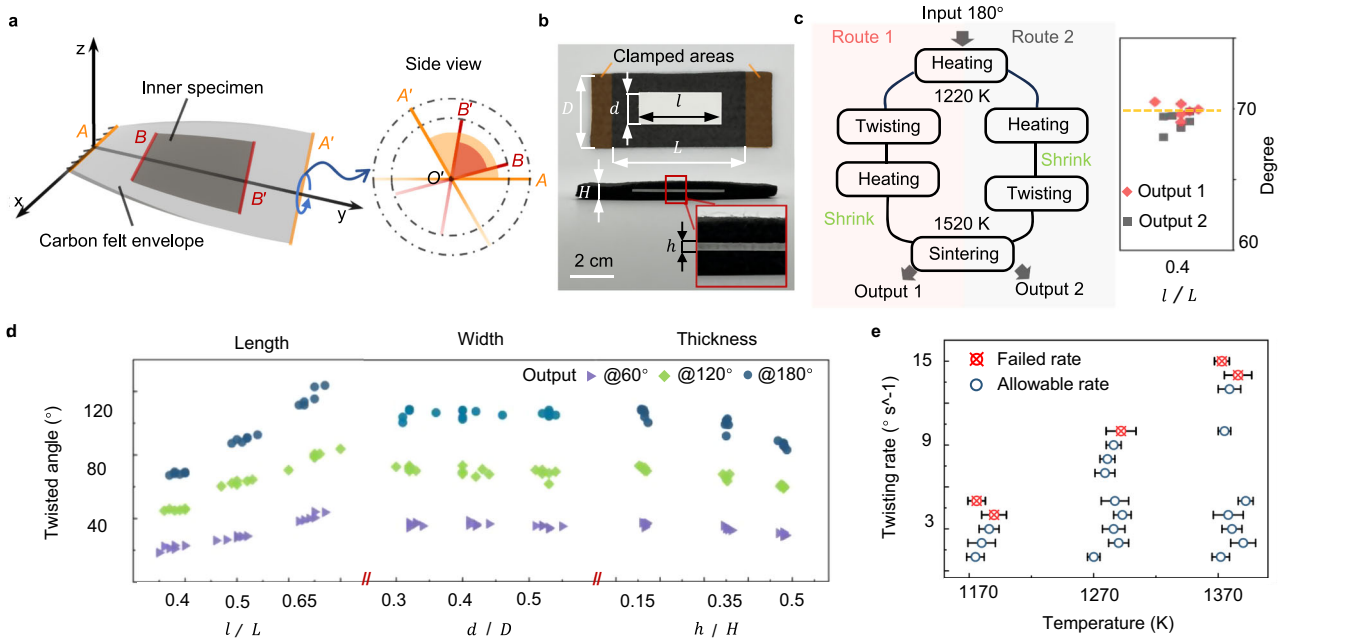

Fig. 3 | Characterization of the USS process by twisting BT ceramics. **a** Schematic illustrations of twisted angles of the carbon felt carrier and enveloped ceramic specimen. **b** Digital images of the BT green compact and the carbon felt heater/carrier. The *L*, *D*, and *H* represent the length, width, and thickness of the carbon felt, respectively. The *l*, *d*, and *h* represent the length, width, and thickness of the ceramic green compact. **c** Processing stability characterization, illustrating that the processing routes have no significant effects on the final shapes of USS specimens. **d** Quantitative study on the shape formation of twisting BT ceramics, where the points denote output angles of samples with different relative lengths, widths, and thicknesses at input angles of 60, 120, and 180 degrees, respectively. The solid lines denote ideal values of output angles. The experimental data show that the relative length is the main geometrical factor affecting (linearly) the final shapes of the twisting ceramics. **e** Twisting rate as a function of processing temperature. The red points represent failed testing speed (too fast). Specifically, the twisting angles of the as-fabricated ceramics cannot reach 95% of the baseline (ideal) values by using this failed twisting rate. The error bar denotes the slight temperature variation during processing.

BT ceramic shows comparable thermal stability (Curie temperature of around 143 °C in Supplementary Fig. 2d) with conventional-sintered bulk BT ceramics[33]. Surprisingly, as shown in Fig. 2f, our rapid fabricated BT ceramics possess superior piezoelectric coefficient (380 pC/N) than most conventional printed[34–38] and bulk BT ceramics[39,40]. The high piezoelectricity of BT ceramic produced by the USS method may originate from (i) proper grain size by short sintering duration[41,42], (ii) good densification by high heating rates[1,43,44]. In Fig. 2g, we highlight that compared with existing complex-shaped ceramic fabrication methods like slip casting[12], ceramic 3D printing method[14], ceramic 4D printing method[45] and the gravity-driven methods[24], the USS method shorten the processing time, showing potential to move ceramic shaping and sintering towards a time-efficient process. The USS process also allows us to freely twist (Supplementary Fig. 3a) and retwist (Supplementary Fig. 3b) the specimens. Note that by adjusting the input power, the temperature profile is programable (Supplementary Fig. 4 and Supplementary Note 2), fitting to the synthesis of other ceramics. The short processing duration and smart heating strategy make the USS method energy-friendly. The electric energy cost for USS method is only 1.06 kilojoules per cubic millimeter for fabricating the twisted ceramics shown in Fig. 2C, whereas conventional furnaces sintering consumes at least 4.69 kilojoules per cubic millimeter (see section "Methods" for the calculations).

Next, we explore the stability and tunability of the USS process by quantitatively studying the mechanisms of the twisting angle formation. To describe the mechanical input, we first in-situ measured the input torque on the connecting shaft between the rotation platform and copper clamps by strain gauges (Supplementary Fig. 5a, b). The measured torques almost equal to 0 N•m (Supplementary Fig. 5c), indicating that the parameters usually used in elastic deformation system may not able to capture the feature of viscous deformation system. Actually, the shape formation during the USS process hinges on the viscous deformation of ceramic powder compacts, which is time-dependent variable and normally described by the rate of deformation[16]. Here, to match the feature of viscous system, we use the twisting rate of the rotation platform as mechanical input for the quantitative study. We use the relative angles between the projections of the two sides (A–A′ and B–B′ in Fig. 3a) of the carbon felts and ceramics to characterize the twisted geometries (see Supplementary Fig. 6 for the angle measurement). Specifically, defining the angle AOA′ and the BOB′ as the input and the output, respectively. Given identical starting materials, twisting rate and the input angles as well as nearly the same thermal treatment (see experiment details in the Supplementary), we reason that three geometrical parameters: relative length *l*/*L*, width *d*/*D*, and thickness *h*/*H* (Fig. 3b) are responsible for the output angle BOB′. Before studying the tunability, we found that processing routes (heating and twisting) nearly have no effects on the final shapes of the twisted BT ceramics. For example, the output angles of specimens fabricated by two processing routes are distributed in similar value region (dash line in Fig. 3c), indicating the robustness of our USS process. For tunability test, all experimental data show that, for each parameter group (columns in Fig. 3d) the output angle increases linearly with the input angle (60°, 120°, and 180°). Interestingly, from Fig. 3d (length) we found that when the inner ceramics are well clamped by the carrier, the values of BOB′ distribute near to the ideal angle values (solid curves in Fig. 3d), which are calculated by multiplying the value of the input angle with the relative length. Note that the ideal output angle is obtained if we assume the clamped specimens follow the shapes of the morphing carbon felts. That is, for instance, for input AOA′ of 180°, the mean values of BOB′ at relative length of 0.5 and 0.65 are 89.8° and 119.3°, respectively ($BOB'_{0.5}/AOA' = 0.499 \approx 0.5$, $BOB'_{0.65}/AOA' = 0.663 \approx 0.65$ see

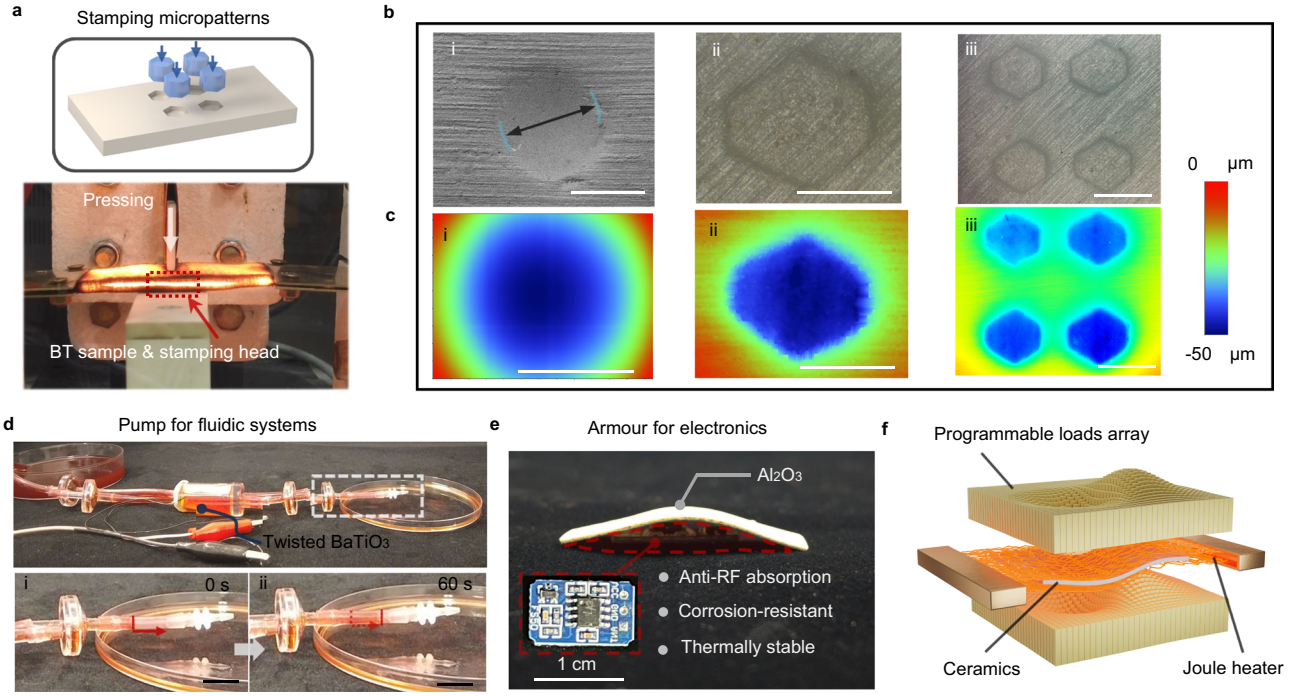

Fig. 4 | Devices produced by the USS process. a Schematic illustration and digital image of stamping micropatterns on ceramics by the USS process. **b** Surface images of BT ceramics with stamped micropatterns including spherical shape, hexagonal shape and prism array, showing the potential of the USS approach in manipulating the surface microstructures of ceramic materials. Scale bar 300 um. **c** The depth distribution of the pressed micropatterns, showing smooth and similar profiles with the corresponding master patterns. Note that the variation in the depth of each unit in the array is caused by the slope of the stamping head during processing. Scale bar 300 um. **d** Application demonstration of the twisted piezoceramic, serving as the actuation part in a pump. The pump is in operation (Supplementary Movie 4). Scale bar 1 cm. **e** Photograph of the arch-shaped alumina ceramic that serves as an armor for electronics. Compared with metals and plastics, the ceramic armors are anti-RF absorption, corrosion-resistant and thermally stable. **f** A design for fabricating ceramic materials in arbitrary shapes that involves a Joule heater and two programmable load arrays for guiding the ceramic sample deform.

Supplementary Note 3 for experiment details). Our experiments (Fig. 3d, width) also show that the final shapes of the twisting ceramics are not sensitive to the width of the specimens. Furthermore, the output twisting angles of thick ceramic compacts are slightly lower than those of thin specimens (Fig. 3d, thickness). These experimental results indicate that the twisting degree of the specimen is tunable and the relative length is the key factor determining the ratio between the output to the input angles.

As a torsional force is applied, the reaction deformation (twisting angle) of the carbon felt envelope (the carrier and heater) could be derived from a torsional plate model (Supplementary Fig. 7). With good force transmission path (Supplementary Fig. 8a), the carbon carrier forces the clamped ceramic green compact deform in a similar modal (bottom left in Supplementary Fig. 7), which explains for the linear changes of the output BOB′ towards the l/L at high level of length ratio. In addition, the centrosymmetric stress distribution in the cross-section (right of Supplementary Fig. 7) indicates that the mechanical driven force has no relation with the relative width (at given length and thickness), causing unsensitivity of the output angle to the value of d/D. The shaping process follows the viscosity-dominated viscoelastic deformation, where the elastic deformation mechanism has little impact on the twisting process. Therefore, the increased torsional constant (bottom right in Supplementary Fig. 7) cannot fully account for the incomplete twisting angles observed in experiments (Fig. 3d). The in-situ observations (Supplementary Fig. 8b) show that in high value of h/H, the carrier cannot closely envelope the ceramic green compacts, causing the unsatisfied driven forces (both in thermal and mechanical) for twisting specimens. Besides, the intensity of the thermal field is also important to the USS process. The main working principle of our USS process relies on the thermal-induced viscosity, a property that is usually described by the deformation rate. Therefore, we use the allowable twisting speed to qualify the fabrication performance of our shaping strategy at different processing temperatures (see Methods for details of the experiments). The results (Fig. 3e) denote that the shaping process can be further speed up by slightly increasing the processing temperature.

Demonstrations of the application potential of the USS process

In addition to forming macroscopic geometries, the USS method also allows for stamping micropatterns on the ceramic materials, as we demonstrated using BT ceramics (Fig. 4a and see Supplementary Movie 3 for the stamping process). To do so, we use zirconia heads with a spherical shape, hexagonal shape and prism array to apply pressures on ceramics, respectively. The viscous body of the BT ceramic (at shaping temperatures) ensures the replication of patterns from stamping heads (Fig. 4b). The smooth scanning profiles (Fig. 4c) match with the master patterns, showing the potential of our approach in manipulating the surface structures of ceramic materials. Note that for stamping the array pattern, the variation (the right map in Fig. 4c) of the depth of each unit originates from the slope of the stamping heads during moving (see Supplementary Fig. 9 and section “Methods” for details). We are able to shape the ceramic powder compacts like kneading plasticines as long as the complex thermomechanical driven force can be applied. The USS-fabricated ceramics in complicated shapes are expected to promote the evolutions of ceramic-based devices. Taking the as-twisted piezoceramics as an example, a demonstration of applying the twisted-shape piezoceramics is a pump for fluidic systems (Fig. 4d). The pump operates through the converse piezoelectric effect (Supplementary Fig. 10 and section “Methods” for the experiment setup). In generating flow, an external electric filed is

applied to drive the inner twisted BT ceramic vibrates (Supplementary Movie 4) and the calculated maximum flowrate is around 0.3 ml/min. To study the working mechanism of the piezoelectric pump, we experimentally and numerically analyzed the vibration of the inner twisted piezoceramic (see Supplementary Note 4 and Supplementary Fig. 11a for the experiment setup). Both the measured displacement results (Supplementary Fig. 11b, c) and simulated displacement distributions (Supplementary Fig. 11d, e) confirm that instead of rotation the vibration modal of the twisted BT ceramic in the piezoelectric pump is similar to a vibrating cantilever beam (Supplementary Movie 5). Besides functional ceramics, our USS approach also facilitates the fabrication of structural ceramic components, for example the arch-shaped alumina armor for protecting or packaging electronics (Fig. 4e). In future works, programmable load arrays may be introduced in our USS system for guiding the ceramic materials deform (Fig. 4f).

Discussion

In summary, we demonstrate how the thermomechanical field engineering namely the USS process shapes brittle piezoceramics while simultaneously keeping their piezoelectric properties, endowing bulk piezoceramics with improved geometrical versatility. The Joule-heated USS process enables the efficient production of complex-shape piezoceramics. Furthermore, the fast sintering and low energy consumption of the USS promotes green manufacturing and carbon neutrality. The demonstration of creating micro patterns on ceramics exhibits the potential of implementing the USS process on a micro-scale. The concept of our USS process is appliable to a broad range of ceramic materials including structural and functional ceramics, because the thermal-induced viscosity exists in various ceramic powder compacts. Despite these promising potentials, there are remaining challenges. 1) The heat transfer modes in the USS method are contact and radiative heating modes and the nonuniform dissipation of the heat cannot be neglected when the dimension of the clamped ceramic is close to the carbon felts. Moreover, the size up of the heater and scale up of the fabrication process are limited by the heat transfer limitations as well as energy efficiency. 2) The appliable geometries of the USS process can hardly match the demands of complex-shape ceramics in various scenario. More intelligent deformation driven system should be integrated to the USS process to provide three-dimensional and precise deformations. 3) Another challenge is exploring the unique deformation models of the as-fabricated piezoceramics in complicated shapes. For example, using the spiral-shape piezoelectric ultrasound transducer to generate spiral-distributed ultrasound fields. The unique application scenario of complex-shape piezoceramics require rational design of configurations, electrode layouts, and driven patterns. Overall, the USS method is expected to promote the development of new 3D ceramic structures and electronics.

Methods

Preparation of the ceramic green compacts

The ceramic powders barium titanate ($BaTiO_3$, Purity: 99.9%, mean particle size: 200 nm) and Alumina (Al_2O_3, Purity: 99.9%, mean particle size: 200 nm) used in the experiments were purchased from Macklin. The polyvinyl alcohol (PVA, purchased from Macklin) binder (4% by weight of powders) was added to the powders. Then, the powders were uniaxially pressed to rectangle green compacts with dimension of 40 mm × 15 mm × 0.4 mm at 25 MPa in a steel mold. The green compacts were debinded at 770 K for 30 mins with heating rate of 10 K/min.

Setup of the USS process

In the Joule heating platform, carbon felts with 60 mm in length, 30 mm in width and 4 mm in thickness (CarbonEnergy Co., Ltd., China) connecting with a DC power supply (KXN 3060D, Zhaoxin power Co., Ltd., China) serve as rapid heating elements, where the temperature profile was regulated by tuning the input current (0–60 A) and voltage (0–30 V). The temperature of the heater and the ceramic samples were measured and recorded via a thermometer (FOTRIC 600 C, Fotric Co., Ltd., China).

As schematically shown in Fig. 2a, b, the carbon stripes were clamped by two copper clamps (also serve as electrodes) that were mechanically fixed onto two rotating platform to transmit torsional deformation. Note that the rotating platforms (RC01RA100-JC, Ruicheng Instrument, China) and vertical moving platform (RC261TA100-GH, Ruicheng Instrument, China) are controlled by a control box connecting with a computer.

Thanks to the ultralow thermal conductivity of Argon (Ar), all USS processes were conducted in an Ar-filled seal box (at room atmospheric pressure) to 1) avoid the oxidation of the carbon felts at high temperature 2) protect the moving platforms, thermometer, and data transmission lines in the box. Besides, to reduce the thermal loss and maintain a stable synthesis atmosphere, several alumina fiber plate insulators were placed around the heating element.

Operation of the USS process

Twisting BT ceramics (Supplementary Movie 1). In a general USS process, take twisting the BT ceramic as a demonstration, the operation is shown below:

1. The green compacts were placed into the carbon felt (inducing an incision with a knife).
2. Turn on the DC power supply and tune the current input (from 0–30 A).
3. After the temperature reaches to around 1370 K, setting the value and twisting rate of the twisting angles in the control port (controlling system in computer). Note that during twisting, the current input may need slight adjustment to maintain the processing temperature.
4. After shaping, further heating the ceramic samples by increasing the current input until the temperature reaches to around 1520 K. Maintaining the temperature (~1520 K) with around 10 seconds for sintering BT ceramics.
5. Reducing the current input to 0 A gradually to avoid the sample crack by suddenly significant temperature fluctuations (for example, directly cut off the current input).

Bending BT ceramics to arch shape (Supplementary Movie 2). For the bending demonstration as shown in Fig. 2e, the sample placement and temperature setup are identical with the aforementioned operation for twisting ceramics. In the step of applying mechanical driven force/deformation, we used an alumina plate (40 mm × 30 mm × 5 mm) fixed onto the vertical moving platform to drive the carbon felt as well as clamped ceramic samples bend against gravitational direction. In this demonstration the moving rate of the alumina plate is 0.3 mm/s.

Stamping micropatterns on BT ceramics (Supplementary Movie 3). Different from the twisting and bending tests, in this demonstration, an alumina block was placed as shown in Supplementary Fig. 9 to support the carbon felts and the clamped ceramic sample during stamping. Printed alumina stamping heads were first placed on the ceramic green compact; and then the ceramic and stamping heads are enveloped in the carbon felts; finally, applying vertical deformation on the carbon felts where the stamping heads are placed. The stamping temperature (~1370 K) and sintering temperature (~1520 K, around 10 s) are identical with twisting BT ceramic by USS approach. Obviously, the stamping processes demonstrated here are far from high-precise and not elegant because the pressing heads and the vertical moving unit are independently separate. One consequence caused by this operation is the nonuniform movement of each unit (for array patterns), and thus resulting in the variation of the depth of each unit (the map iii in Fig. 4c).

Setup and operation of pumping flows by the twisted BT ceramic (Supplementary Movie 4)

The twisted angle of the BT ceramic in the pump is around 100 degree. After polarization, as shown in Supplementary Fig. 10c, the twisted ceramic sample was first fixed in the 3D printed tube by using glue (Ergo 1690, Switzerland). A signal generator (DG1022Z, RIGOL, China) combined with a power amplifier (E01.A2, Coremorrow, China) were used to generate AC voltage input (Supplementary Fig. 10). The inner twisted BT ceramic converts the AC voltage input to mechanical vibration, slapping the silicone oil (red color) in the tube. Note that two check valves were connected with the tube for guiding the flow direction of the silicone oil. In this demonstration (Fig. 4d and Supplementary Movie 4), the amplitude of the input voltage is 200 V and the frequency is 3000 Hz. The inner and outer diameter of the soft pipe are 2 mm and 3 mm, respectively. From the operation video (Supplementary Movie 4) and Fig. 4d, we can calculate that the maximum flowrate is around 0.3 ml/min.

Material characterization

The densities of sintered BT ceramics were measured through Archimedes' method. The microstructures of the as-sintered ceramics were observed with scanning electron microscopy (SEM; FEI Quanta 450). Elemental mapping (EDS) was derived from energy dispersive spectrometer (Oxford Instruments, INCA Energy 200). X-ray diffraction (Rigaku SmartLab) was employed for measuring the phase structures of the sintered BT ceramics with scan speed of 4° per minute. For measuring the ferroelectric properties of the as-fabricated piezoceramics, silver electrodes were deposited onto the surface of cut specimens with magnetron sputtering (Q150TS). The ceramic samples were poled at electric field of 3 kV/mm at room temperature in silicone oil. The quasi-static piezoelectric meter was used to measure the piezoelectric constants (YE2730A d33 meter). The as-synthesized BT ceramics were carefully polished via polishing machine (UNIPOL-830, Kejing Auto-instrument Co., Ltd, China) in the form of slice with thickness of around 0.1 mm for ferroelectric and electro-strain behavior measurement. The ferroelectric hysteresis loop and the strain–electric field curve were tested by ferroelectric instrument (CPE1801, PolyK Technologies, USA). Temperature dependence of the relative dielectric constant and corresponding dielectric loss tanδ were detected by a high-temperature dielectric property test system with heating rate of 2 °C/min at frequency of 1 kHz (DPTS-RT-600, Wuhan Yanhe Technology Co., Ltd). The twisting angles of the samples listed in Fig. 3d were measured as shown in Supplementary Fig. 6, specifically, using a high-definition camera to record the side photograph of these twisted ceramics. Note that the camera was vertically placed above ceramic samples and focused on the central point of the side of each twisted specimen.

Calculation of the electric energy consumption

The formation and regulation of the thermal field in the USS method relies on the state-of-the-art Joule heating technique, which significantly shorten the processing time and save the requiring electric energy cost. As shown in Supplementary Fig. 4d, the input power is approximately 600 W for maintaining the processing temperature of 1400 K. To illustrate the advantage of the USS method in low energy consumption, we calculate and compare the electric energy cost of our USS method with conventional ceramic fabrication method using. Note that in this calculation we simplified the relation between the power input and the temperature is linear without considering other potential disturbances like the thermal loss and efficiency attenuation. The energy consumption is calculated by the equation below:

$$E_{sum} = \frac{T_p}{T_a} \cdot P \cdot t \quad (1)$$

where E_{sum} denotes the energy consumption; T_p and T_a represent the processing temperature and the maximum allowable temperature of the furnace, respectively, P is the rated power of the furnace and t is the processing time.

Also, in this comparison of electric energy cost, we eliminate the effect of the processing capacity of the two methods by dividing the total volumes the allowable number of processing samples in one processing cycle. Specifically, using kilojoule per cubic millimeter to describe the energy consumption of the two methods. The electric energy cost is thus calculated as:

$$E_{cos} = \frac{E_{sum}}{n \bullet V_{vol}} \quad (2)$$

where E_{cos}, n and V_{vol} denote the electric energy cost, the allowable number of processing samples and volume of the sample.

The furnace (KSL-1400X, Kejing Co., Ltd, China) used for debinding in this work was selected. This choice is not only due to the fact that the majority of ceramics in our group have been synthesized using this furnace, but also because this bench-size furnace is widely available and commonly used in the market. The main parameters of the furnace: 1) maximum temperature is 1400 temperature degree with duration less than 30 min; 2) the allowable long-time processing temperature is 1300 temperature degree; 3) the rated power of this furnace is 5.2 kW; 4) maximum heating rate is 10 temperature degree per minute. We list the processing routes and the energy consumption in Supplementary Table 1.

Data availability

All data are available in the main text or the supplementary materials. Source data are provided with this paper.

References

1. Wang, C. et al. A general method to synthesize and sinter bulk ceramics in seconds. *Science* **368**, 521–526 (2020).
2. Penilla, E. H. et al. Ultrafast laser welding of ceramics. *Science* **365**, 803–808 (2019).
3. Bargardi, F. L., Le Ferrand, H., Libanori, R. & Studart, A. R. Bio-inspired self-shaping ceramics. *Nat. Commun.* **7**, 1–8 (2016).
4. Wang, B. et al. Woodpecker-mimic two-layer band energy harvester with a piezoelectric array for powering wrist-worn wearables. *Nano Energy* **89**, 106385 (2021).
5. Yang, Z., Zhou, S., Zu, J. & Inman, D. High-performance piezoelectric energy harvesters and their applications. *Joule* **2**, 642–697 (2018).
6. Liu, S. et al. 3D conformal fabrication of piezoceramic films. *Adv. Sci.* **9**, 1–10 (2022).
7. Shan, Y. et al. Three-dimensional piezoceramic sheets via mold-assisted sintering as 3D energy transducers. *Mater. Today* **68**, 74–83 (2023).
8. Hu, H. et al. Stretchable ultrasonic transducer arrays for three-dimensional imaging on complex surfaces. *Sci. Adv.* **4**, eaar3979 (2018).
9. Janssen, R., Scheppokat, S. & Claussen, N. Tailor-made ceramic-based components-Advantages by reactive processing and advanced shaping techniques. *J. Eur. Ceram. Soc.* **28**, 1369–1379 (2008).
10. Bouville, F. et al. Strong, tough and stiff bioinspired ceramics from brittle constituents. *Nat. Mater.* **13**, 508–514 (2014).
11. Ortiz, A. L., Candelario, V. M., Moreno, R. & Guiberteau, F. Near-net shape manufacture of B4C–Co and ZrC–Co composites by slip casting and pressureless sintering. *J. Eur. Ceram. Soc.* **37**, 4577–4584 (2017).
12. Tallon, C., Limacher, M. & Franks, G. V. Effect of particle size on the shaping of ceramics by slip casting. *J. Eur. Ceram. Soc.* **30**, 2819–2826 (2010).

13. Huachen, C. et al. Design and printing of proprioceptive three-dimensional architected robotic metamaterials. *Science* **376**, 1287–1293 (2022).
14. Lu, H. et al. 3D Printing and processing of miniaturized transducers with near-pristine piezoelectric ceramics for localized cavitation. *Nat. Commun.* **14**, 1–11 (2023).
15. Liu, C., Du, Q., Zhang, C., Wu, J. & Zhang, G. Fabrication and properties of BaTiO 3 ceramics via digital light processing for piezoelectric energy harvesters. *Addit. Manuf.* **56**, 102940 (2022).
16. Lee, S., Messing, G. L. & Green, D. J. Bending creep test to measure the viscosity of porous materials during sintering. *J. Am. Ceram. Soc.* **86**, 877–882 (2003).
17. Gibeling, J. C. Creep deformation of metals, polymers, ceramics, and composites. in *Mechanical Testing and Evaluation ASM Handbook*, Vol. 8, 363–368 (ASM International, 2000).
18. Sherby, O. D. & Burke, P. M. Mechanical behavior of crystalline solids at elevated temperature. *Prog. Mater. Sci.* **13**, 323–390 (1968).
19. Hiraga, K. et al. High-strain-rate superplasticity in oxide ceramics. *Sci. Technol. Adv. Mater.* **8**, 578–587 (2007).
20. Maehara, Y. & Langdon, T. G. Superplasticity in ceramics. *J. Mater. Sci.* **25**, 2275–2286 (1990).
21. Chokshi, A. H. Diffusion creep in oxide ceramics. *J. Eur. Ceram. Soc.* **22**, 2469–2478 (2002).
22. Ding, J. -L., Liu, K. C., More, K. L. & Brinkman, C. R. Creep and creep rupture of an advanced silicon nitride ceramic. *J. Am. Ceram. Soc.* **77**, 867–874 (1994).
23. Ashby, M. F. A first report on deformation-mechanism maps. *Acta Met.* **20**, 887–897 (1972).
24. Shan, Y. et al. A gravity-driven sintering method to fabricate geometrically complex compact piezoceramics. *Nat. Commun.* **12**, 1–7 (2021).
25. Schoenberg, S. E., Green, D. J. & Messing, G. L. Effect of green density on the thermomechanical properties of a ceramic during sintering. *J. Am. Ceram. Soc.* **89**, 2448–2452 (2006).
26. Cai, P. Z., Messing, G. L. & Green, D. L. Determination of the mechanical response of sintering compacts by cyclic loading dilatometry. *J. Am. Ceram. Soc.* **80**, 445–452 (1997).
27. Ping, W. et al. Printable, high-performance solid-state electrolyte films. *Sci. Adv.* **6**, eabc8641 (2020).
28. Yao, Y. et al. High-entropy nanoparticles: synthesis-structure-property relationships and data-driven discovery. *Science* **376**, eabn3103 (2022).
29. Dong, Q., Yao, Y., Cheng, S., Alexopoulos, K. & Gao, J. Programmable heating and quenching for non-equilibrium thermochemical synthesis. *Nature* **605**, 470–476 (2022).
30. Dong, Q. et al. Depolymerization of plastics by means of electrified spatiotemporal heating. *Nature* **616**, 488–494 (2023).
31. Dong, Q. et al. A general method for regenerating catalytic electrodes. *Joule* **4**, 2374–2386 (2020).
32. Wang, X. et al. Ultrahigh-temperature melt printing of multi-principal element alloys. *Nat. Commun.* **13**, 1–8 (2022).
33. Karaki, T., Yan, K. & Adachi, M. Barium titanate piezoelectric ceramics manufactured by two-step sintering. *Jpn. J. Appl. Phys.* **46**, 7035–7038 (2007).
34. Kim, K. et al. 3D optical printing of piezoelectric nanoparticle-polymer composite materials. *ACS Nano* **8**, 9799–9806 (2014).
35. Takeuchi, M. et al. $BaTiO_3$ particle-size dependence of ferroelectricity in $BaTiO_3$/polymer composites. *Jpn. J. Appl. Phys.* **32**, 4272 (1993).
36. Zeng, Y. et al. 3D-printing piezoelectric composite with honeycomb structure for ultrasonic devices. *Micromachines* **11**, 713 (2020).
37. Choi, W., Choi, K., Yang, G., Kim, J. C. & Yu, C. Improving piezoelectric performance of lead-free polymer composites with high aspect ratio BaTiO3 nanowires. *Polym. Test.* **53**, 143–148 (2016).
38. Capsal, J. F., Dantras, E., Laffont, L., Dandurand, J. & Lacabanne, C. Nanotexture influence of BaTiO3 particles on piezoelectric behaviour of PA 11/BaTiO3 nanocomposites. *J. Non Cryst. Solids* **356**, 629–634 (2010).
39. Chen, Z. et al. 3D printing of piezoelectric element for energy focusing and ultrasonic sensing. *Nano Energy* **27**, 78–86 (2016).
40. Kim, H. et al. Fabrication of bulk piezoelectric and dielectric BaTiO 3 ceramics using paste extrusion 3D printing technique. *J. Am. Ceram. Soc.* **102**, 3685–3694 (2019).
41. Huan, Y., Wang, X., Fang, J. & Li, L. Grain size effect on piezoelectric and ferroelectric properties of $BaTiO_3$ ceramics. *J. Eur. Ceram. Soc.* **34**, 1445–1448 (2014).
42. Yan, K., Chen, X., Wang, F. & Zhu, K. Large piezoelectricity and high transparency in fine-grained $BaTiO_3$ ceramics. *Appl. Phys. Lett.* **116**, 082902 (2020).
43. Zhang, Y., Nie, J., Chan, J. M. & Luo, J. Probing the densification mechanisms during flash sintering of ZnO. *Acta Mater.* **125**, 465–475 (2017).
44. Ji, W. et al. Ultra-fast firing: effect of heating rate on sintering of 3YSZ, with and without an electric field. *J. Eur. Ceram. Soc.* **37**, 2547–2551 (2017).
45. Liu, G., Zhao, Y., Wu, G. & Lu, J. Origami and 4D printing of elastomer-derived ceramic structures. *Sci. Adv.* **4**, 1–11 (2018).

Acknowledgements

The work described in this paper was supported by the Hong Kong Research Grants Council (GRF Project No. 11212021 and No. 11210822), and the Innovation and Technology Fund (Project No. ITS/065/20; GHP/096/19SZ) from Innovation and Technology Commission of Hong Kong Special Administrative Region. We thank Mr. Yi Zheng's supports on the deformation simulation of vibrating twisted piezoceramics. We also appreciate Mr. Riran Liang's help on measuring the torque of the connecting shaft.

Author contributions

Y.S., X.L., W.Z. and Z.Y. conceived the project and designed the studies. Y.S., X.L., and W.Z. performed experiments and analyzed the experimental data. Y.S., W.Z. and X.L. worked on the construction of the processing platform, with assistance from W.Z., X.L., X.Y., Y.W., Z.Z., S.L., and X.X. in materials characterization. Y.S., X.L. and Z.Y. composed the manuscript. All authors discussed the results and commented on the manuscript. Y.S., X.L. and W.Z. contribute equally to this study and share the first authorship.

Competing interests

The authors declare no competing interests.

Additional information

Supplementary information The online version contains supplementary material available at https://doi.org/10.1038/s41467-024-54393-w.

Correspondence and requests for materials should be addressed to Zhengbao Yang.

Peer review information *Nature Communications* thanks Qi Zhao and the other, anonymous, reviewer(s) for their contribution to the peer review of this work. A peer review file is available.